

## Effect of time-delay and dissipative coupling on amplitude death in coupled thermoacoustic oscillators

Nevin Thomas, Sirshendu Mondal, Samadhan A. Pawar, and R. I. Sujith

Citation: *Chaos* **28**, 033119 (2018); doi: 10.1063/1.5009999

View online: <https://doi.org/10.1063/1.5009999>

View Table of Contents: <http://aip.scitation.org/toc/cha/28/3>

Published by the [American Institute of Physics](#)

---

### Articles you may be interested in

[Amplitude death model exhibits control of thermoacoustic oscillations](#)

*Scilight* **2018**, 130004 (2018); 10.1063/1.5030654

[Synchronous behaviour of two interacting oscillatory systems undergoing quasiperiodic route to chaos](#)

*Chaos: An Interdisciplinary Journal of Nonlinear Science* **27**, 103119 (2017); 10.1063/1.4991744

[Introduction to Focus Issue: Time-delay dynamics](#)

*Chaos: An Interdisciplinary Journal of Nonlinear Science* **27**, 114201 (2017); 10.1063/1.5011354

[Prediction of flow dynamics using point processes](#)

*Chaos: An Interdisciplinary Journal of Nonlinear Science* **28**, 011101 (2018); 10.1063/1.5016219

[Dynamic behavior of combustion instability in a cylindrical combustor with an off-center installed coaxial injector](#)

*Chaos: An Interdisciplinary Journal of Nonlinear Science* **28**, 033111 (2018); 10.1063/1.5025480

[Acoustic-hydrodynamic-flame coupling—A new perspective for zero and low Mach number flows](#)

*Physics of Fluids* **29**, 046102 (2017); 10.1063/1.4981784

---

Welcome to a

Smarter Search 

PHYSICS  
TODAY

with the redesigned  
*Physics Today Buyer's Guide*

Find the tools you're looking for today!

# Effect of time-delay and dissipative coupling on amplitude death in coupled thermoacoustic oscillators

Nevin Thomas, Sirshendu Mondal,<sup>a)</sup> Samadhan A. Pawar, and R. I. Sujith  
*Indian Institute of Technology Madras, Chennai 600036, India*

(Received 21 October 2017; accepted 26 February 2018; published online 27 March 2018)

We here systematically investigate amplitude death (AD) phenomenon in a thermoacoustic system using a mathematical model of coupled prototypical thermoacoustic oscillators, the horizontal Rijke tubes. AD has recently been identified as a relatively simple phenomenon, which can be exploited to stop the unwanted high amplitude pressure oscillations resulting from the occurrence of thermoacoustic instability. We examine the effect of time-delay and dissipative couplings on a system of two Rijke tubes when they are symmetrically and asymmetrically coupled. The regions where appropriate combinations of delay time, detuning, and the strengths of time-delay and dissipative coupling lead to AD are identified. The relative ease of attaining AD when both the couplings are applied simultaneously is inferred from the model. In the presence of strong enough coupling, AD is observed even when the oscillators of dissimilar amplitudes are coupled, while a significant reduction in the amplitudes of both the oscillators is observed when the coupling strength is not enough to attain AD. *Published by AIP Publishing.*

<https://doi.org/10.1063/1.5009999>

Most of the practical combustors used in rockets and gas turbine engines are susceptible to thermoacoustic instabilities. In simple terms, thermoacoustic instability may occur when the heat release rate fluctuations from a heat source in a confinement are in phase with the acoustic pressure fluctuations, and in turn, amplify them. These high amplitude pressure oscillations have many adverse effects such as reduction in the lifetime of the engines and structural damage. Many control techniques, both passive and active, have been implemented in the past to suppress these undesired oscillations. Here, we study an approach based on amplitude death (AD) phenomenon to suppress these oscillations in a system of coupled thermoacoustic oscillators. AD is a general outcome in coupled oscillators, wherein individual oscillators cease to oscillate when coupled appropriately. The possibility of suppression of high amplitude oscillations in coupled thermoacoustic engines using the AD phenomenon has recently been explored. However, the physical mechanisms leading to limit cycle oscillations in thermoacoustic engines are significantly different from those which lead to thermoacoustic instability in the system we consider. In this paper, we examine the effects of time-delay and dissipative couplings on the AD behaviour of a system of two coupled horizontal Rijke tubes—prototypical thermoacoustic oscillators. The combinations of parameters such as coupling strength, delay time, detuning, and heater power at which bifurcation to AD happens are determined, and the regions of AD in various parameter planes are identified. Interesting results are also obtained when two oscillators of different amplitudes are coupled, and when asymmetry is introduced in the coupling.

## I. INTRODUCTION

Coupled nonlinear oscillators exhibit a range of interesting phenomena such as synchronization and oscillation quenching, depending on the dynamics of the system and the manner in which the coupling is organized.<sup>1</sup> Generally, weak coupling leads to synchronization or phase locking,<sup>2,3</sup> while strong coupling will have effects on amplitude, leading to oscillation quenching.<sup>4,5</sup> The oscillation quenching phenomenon has two structurally different manifestations, namely, amplitude death (AD) and oscillation death (OD). When the parameter values of a system of coupled oscillators are appropriate to bring about AD, the oscillations of the individual oscillators cease, and subsequently all the oscillators return to the same steady state of the system.<sup>6</sup> On the contrary, oscillation death (OD) results from the symmetry breaking of the system and the individual oscillators occupy altered steady states which are different from the original steady state of the system.<sup>7</sup> Although both phenomena have been widely observed in nature and have many useful applications, in this paper, we restrict our study to the occurrence of AD in coupled thermoacoustic oscillators exhibiting limit cycle behaviour.

The first instance of AD was reported by Rayleigh in a system of two organ pipes positioned side by side.<sup>8</sup> He observed that, when the two pipes were kept close by, their effect on each other caused the sound from both to die down, whereas each of them sounded with its own frequency when kept far away, free from the influence of the other pipe. Recent studies by Abel *et al.*<sup>9,10</sup> made use of experiments and mathematical models to explain this phenomenon based on synchronization theory. Subsequently, AD has been experimentally observed in a variety of systems such as electrically coupled chemical oscillators,<sup>11</sup> thermo-kinetic oscillators,<sup>12</sup> and many coupled electronic circuits.<sup>5,13</sup> Different

<sup>a)</sup>Electronic mail: sirshendumondal13@gmail.com

types of couplings including dissipative, time-delay, dynamic, conjugate, and nonlinear are experimentally found capable of leading coupled oscillatory systems to a state of AD.<sup>14</sup> With proper control strategies, we can avoid unwanted oscillations in certain systems by inducing AD; while, in other instances where oscillations have to be maintained (e.g., pulse combustors<sup>15,16</sup>), we can ensure that the system never reaches the AD state. AD phenomenon finds applications in fields such as neuronal disorders, laser applications, and meteorological phenomena.<sup>14</sup> From all these studies, we can infer that AD is a general outcome in coupled nonlinear oscillator systems with many important applications.

In this paper, we investigate the occurrence of AD in a mathematical model of thermoacoustic oscillators coupled through time-delay and dissipative couplings. Generally, a thermoacoustic system consists of a heat source (or flame) confined in a duct. Thermoacoustic engine is another common system where thermal power is converted into acoustic power, resulting in high-amplitude pressure oscillations.<sup>17</sup> A typical thermoacoustic engine consists of a porous stack, installed between hot and cold heat exchangers, inside a tube. The pressure disturbances in the working gas are amplified because of the temperature gradient across the stack, which results in the generation of a loud sound when a steady state is reached.<sup>17,18</sup> In contrast, thermoacoustic instabilities arise from a positive interplay between the acoustic field of the duct and the heat release rate fluctuations from the flame, resulting in the system dynamics reaching a state of very high-amplitude oscillations.<sup>19</sup> The physical mechanisms underlying thermoacoustic instability, resulting from combustion driven oscillations,<sup>20</sup> is markedly different from what happens inside a thermoacoustic engine. The importance of thermoacoustic instability can be inferred from the fact that it has been observed in systems ranging from high performance propulsive systems such as rockets and aircraft engines to power generation units such as gas turbine engines and boilers.<sup>21,22</sup> Very often, adverse effects such as flame flashback and blowout of the flame<sup>23</sup> happen due to thermoacoustic instability. In addition to this, high-amplitude pressure oscillations cause large levels of vibrations which can lead to a reduction in the lifetime of engines or cause serious structural damage.<sup>20</sup> Therefore, prediction and control of these high amplitude oscillations are of primary importance in real engines.<sup>24,25</sup>

Hitherto, the high amplitude pressure oscillations observed during thermoacoustic instability were suppressed using passive controls such as the installation of acoustic dampers, liners, baffles, and changing the flame anchoring position.<sup>20,26</sup> Despite the simplicity of these passive control approaches, they are effective only over a limited range of operating conditions. A different approach involves active control strategies such as feedback control<sup>27</sup> and adaptive control<sup>28</sup> which could suppress the undesired thermoacoustic instabilities using actively functioning electro-mechanical devices. However, in active control, analyzing the pressure fluctuations and actively taking the necessary steps to stop thermoacoustic instability requires complicated electro-mechanical feedback systems, which limits the practical applicability of such control methods in actual gas turbine

engines.<sup>29</sup> Another approach for damping these thermoacoustic oscillations is to use external periodic forcing<sup>30,31</sup> (open-loop control), which also falls short of practicality because of the difficulty in installing the actuators in real combustors. Recently, Biwa *et al.*<sup>32</sup> made use of a simple approach based on AD phenomenon to suppress the pressure oscillations in coupled thermoacoustic engines, wherein they coupled two such systems using a needle valve (dissipative coupling) and a vinyl tube (time-delay coupling). For appropriate values of coupling parameters, they observed complete suppression of oscillations or AD in both the engines.

Almost all of the previous studies on thermoacoustic instabilities considered the suppression of oscillations in isolated systems. Suppression of these oscillations in coupled systems is not a much explored field which can be of significance in many practical systems, for instance, can and can-annular type combustors.<sup>33</sup> Although, Biwa *et al.*<sup>32</sup> provides experimental evidence of AD in thermoacoustic engines, the system they studied does not involve mean flow and physically has very little in common with thermoacoustic instability observed in practical combustors. Further, their modelling was based on simple equations of coupled Van der Pol oscillators, which do not adequately capture the dynamics of a practical thermoacoustic system. Further, in majority of the previous studies,<sup>14</sup> the focus was on symmetric coupling; however, in practice, such an ideal scenario is unlikely to exist. Therefore, we study the effect of asymmetrical coupling on AD behaviour of thermoacoustic systems. Also, the oscillations inside similar (dimensionally) practical combustors operating at the same conditions may not be identical owing to the inhomogeneities involved in real systems. Hence, we further investigate the prospect of achieving AD or at least suppressing the oscillations to a good extent in such systems.

To that end, we adopt a prototypical model of a thermoacoustic oscillator, known as horizontal Rijke tube,<sup>34</sup> and perform the first systematic theoretical investigation on the effects of the two different types of couplings (time-delay and dissipative) applied separately and simultaneously on such systems. We observe the response of the system to varying coupling parameters and note the bifurcation points where the dynamics of both the oscillators transition from limit cycle to AD. While dissipative coupling can lead to AD only if there is a sufficient difference in the natural frequencies (detuning) of the two oscillators,<sup>35</sup> time-delay coupling of sufficient strength with appropriate delay can bring about AD even in a system of two identical oscillators.<sup>5</sup> Simultaneous application of the two couplings leads the coupled thermoacoustic oscillators to reach AD state more easily (with a lesser coupling strength). We also establish that the increased heater power or equivalently increased amplitude of oscillations requires higher coupling strength for achieving AD in the same system. Further, the effect of asymmetry on the coupling parameters required to achieve AD is noted. Results from the model also indicate that AD or at least a significant reduction in amplitude is possible even in a system of two Rijke tube oscillators with considerably different amplitudes.

## II. MODEL FOR COUPLED RIJKE TUBE OSCILLATORS

The prototypical thermoacoustic system we use here is the horizontal Rijke tube. It is a horizontal duct with a concentrated heat source (a heated cylinder in the model used here). The Rijke tube oscillator was often chosen to study the intricacies of thermoacoustic instabilities in the past,<sup>25,34,36,37</sup> because of its analytical tractability.

In this study, we build on the model developed by Balasubramanian and Sujith.<sup>34</sup> The linearized momentum [Eq. (1)] and energy [Eq. (2)] equations for the acoustic field, neglecting the effect of mean flow (zero Mach number approximation) and mean temperature gradient in the duct, are given as<sup>34</sup>

$$\bar{\rho} \frac{\partial \tilde{u}'}{\partial \tilde{t}} + \frac{\partial \tilde{p}'}{\partial \tilde{x}} = 0, \quad (1)$$

$$\frac{\partial \tilde{p}'}{\partial \tilde{t}} + \gamma \bar{p} \frac{\partial \tilde{u}'}{\partial \tilde{x}} = (\gamma - 1) \dot{\tilde{Q}}' \delta(\tilde{x} - \tilde{x}_f). \quad (2)$$

In this model,  $\tilde{x}$  is the distance along the axial direction,  $\tilde{x}_f$  is the location of the heat source,  $\tilde{t}$  is the time,  $\tilde{u}'$  is the acoustic velocity,  $\tilde{p}'$  is the acoustic pressure,  $\bar{\rho}$  and  $\gamma$  are the mean density and the ratio of specific heats of the medium, respectively, and  $\dot{\tilde{Q}}'$  is the heat release rate fluctuations per unit area due to the heated cylinder. Dirac delta ( $\delta$ ) function is used to capture the compactness of the heat source.

The pressure ( $\tilde{p}$ ) at both ends of the duct are equal to the ambient pressure ( $\bar{p}$ ). Therefore, the acoustic pressure fluctuations ( $\tilde{p}'$ ) at the boundaries are negligible, as  $\tilde{p}' = \tilde{p} - \bar{p} = 0$ . As a consequence, we can impose the boundary conditions as  $\tilde{p}' = 0$  at both ends of the duct. Variables in Eqs. (1) and (2) are non-dimensionalized as follows:

$$x = \frac{\tilde{x}}{l}; \quad t = \frac{\tilde{t}}{l/c_0}; \quad u' = \frac{\tilde{u}'}{u_0}; \quad p' = \frac{\tilde{p}'}{\bar{p}}; \quad (3)$$

$$\dot{Q}' = \frac{\dot{\tilde{Q}}'}{c_0 \bar{p}}; \quad M = \frac{u_0}{c_0}. \quad (4)$$

Variables with tilde are dimensional and those without tilde are non-dimensional. Here,  $l$  is the length of the duct,  $u_0$ , and  $\bar{p}$  are the steady state velocity, pressure, and temperature of the flow, respectively,  $c_0$  is the speed of sound, and  $M$  is the Mach number of the mean flow.

After non-dimensionalizing and adding a damping term [ $\zeta p'$  in Eq. (2), where  $\zeta$  is the damping coefficient], the governing equations take the following form:<sup>37</sup>

$$\gamma M \frac{\partial u'}{\partial t} + \frac{\partial p'}{\partial x} = 0, \quad (4)$$

$$\frac{\partial p'}{\partial t} + \gamma M \frac{\partial u'}{\partial x} + \zeta p' = (\gamma - 1) \dot{Q}' \delta(x - x_f). \quad (5)$$

The heat release rate in the duct is modelled using a modified form of King's law.<sup>38,39</sup> This correlation quantifies the quasi-steady heat transfer from a heated cylinder to the flow around it. The thermal inertia of the heat transfer in the medium is captured by a parameter time lag ( $\tau_1$ ). Therefore, an empirical model was suggested in which the heat release

rate fluctuations are written in terms of the acoustic velocity fluctuations (*i.e.*,  $u'_f(t - \tau_1)$ ) observed at the heater location,  $x_f$ , and with a delay ( $\tau_1$ ) as<sup>37,39</sup>

$$\dot{Q}'(t) = \frac{2L_w(T_w - \bar{T})}{S\sqrt{3}c_0\bar{p}} \sqrt{\pi\lambda C_v u_0 \bar{p} l_c} \times \left[ \sqrt{\left| \frac{1}{3} + u'_f(t - \tau_1) \right|} - \sqrt{\frac{1}{3}} \right], \quad (6)$$

where  $l_c$ ,  $L_w$ , and  $T_w$  are the radius, length, and temperature of the heater wire, respectively,  $S$  is the cross sectional area of the duct,  $\bar{T}$  is the steady state temperature of the flow,  $\lambda$ ,  $C_v$  are thermal conductivity and specific heat at constant volume, respectively, of the medium within the duct.

Substituting Eq. (6) in the energy equation, Eq. (5), we obtain<sup>37</sup>

$$\frac{\partial p'}{\partial t} + \gamma M \frac{\partial u'}{\partial x} + \zeta p' = (\gamma - 1) \frac{2L_w(T_w - \bar{T})}{S\sqrt{3}c_0\bar{p}} \sqrt{\pi\lambda C_v u_0 \bar{p} l_c} \times \left[ \sqrt{\left| \frac{1}{3} + u'_f(t - \tau_1) \right|} - \sqrt{\frac{1}{3}} \right] \delta(x - x_f). \quad (7)$$

The set of partial differential equations (PDE) given by Eq. (4) and Eq. (7) can be reduced to ordinary differential equations (ODE) using the Galerkin technique.<sup>40</sup> To that end, velocity ( $u'$ ) and pressure ( $p'$ ) fluctuations in the duct are written in terms of basis functions or the Galerkin modes.<sup>34</sup> These basis functions are nothing but the natural acoustic modes of the duct in the absence of heat release. These functions form a complete basis and also satisfy the boundary conditions ( $p'(0, t) = 0$ ;  $p'(1, t) = 0$ ). The basis functions for  $u'$  and  $p'$  can be written as follows:

$$u' = \sum_{j=1}^N \eta_j \cos(j\pi x), \quad (8)$$

$$p' = - \sum_{j=1}^N \dot{\eta}_j \frac{\gamma M}{j\pi} \sin(j\pi x). \quad (9)$$

Here,  $\eta_j$  and  $\dot{\eta}_j$  correspond to the time-varying coefficients of the acoustic velocity ( $u'$ ) and the acoustic pressure ( $p'$ ) in the Galerkin expansion, respectively, and  $N$  represents the number of Galerkin modes considered. In this study, we choose first ten modes, since addition of further modes brought about only negligible improvement to the solution.<sup>37</sup>

The following ODEs are obtained by substituting the expansions for  $u'$  [Eq. (8)] and  $p'$  [Eq. (9)] into the PDEs given in Eqs. (4) and (7) and then projecting along the basis functions<sup>34</sup>

$$\frac{d\eta_j}{dt} = \dot{\eta}_j, \quad (10)$$

$$\frac{d\dot{\eta}_j}{dt} + 2\zeta_j \omega_j \dot{\eta}_j + \omega_j^2 \eta_j = -j\pi K \left[ \sqrt{\left| \frac{1}{3} + u'_f(t - \tau_1) \right|} - \sqrt{\frac{1}{3}} \right] \sin(j\pi x_f), \quad (11)$$

where

$$u'_f(t - \tau_1) = \sum_{j=1}^N \eta_j(t - \tau_1) \cos(j\pi x), \quad (12)$$

and  $\omega_j = j\pi$  is the non-dimensional angular frequency of the  $j^{\text{th}}$  duct mode. The coefficient of the second term on the left-hand side of Eq. (11),  $2\zeta_j\omega_j\dot{\eta}_j$ , represents the frequency dependent damping,<sup>36,41,42</sup> where  $\zeta_j$  can be written as

$$\zeta_j = \frac{1}{2\pi} \left[ c_1 \frac{\omega_j}{\omega_1} + c_2 \sqrt{\frac{\omega_1}{\omega_j}} \right]. \quad (13)$$

Here,  $c_1$  and  $c_2$  are the damping coefficients, values of which determine the amount of damping in the system. The values of  $c_1$  and  $c_2$  are chosen as 0.1 and 0.06, respectively, for all the simulations in this study. These values are chosen such that it conforms to the cold decay rate calculated from experiments.<sup>43</sup> The value of  $x_f$  is chosen to be 0.25 ( $=l/4$ ), as it is the most favourable location for the onset of thermoacoustic instability.<sup>36</sup>

In Eq. (11),  $K$  represents the non-dimensional heater power which is defined as

$$K = \frac{4(\gamma - 1)L_w(T_w - \bar{T})}{\gamma M c_0 \bar{\rho} S \sqrt{3}} \sqrt{\pi \lambda C_v u_0 \bar{\rho} l c}. \quad (14)$$

When the value of  $K$  is increased beyond a critical value ( $K_{Hopf} = 0.62$ ), the system undergoes a Hopf bifurcation, wherein the oscillations in the system grow and saturate at a high amplitude value [Fig. 1(a)]. This is the state of limit cycle oscillations (LCO). The waveform and amplitude spectrum of the acoustic pressure signal corresponding to  $K = 0.75$  are shown in Figs. 1(b) and 1(c), respectively. At LCO, the system oscillates with a constant amplitude [Fig. 1(b)] and

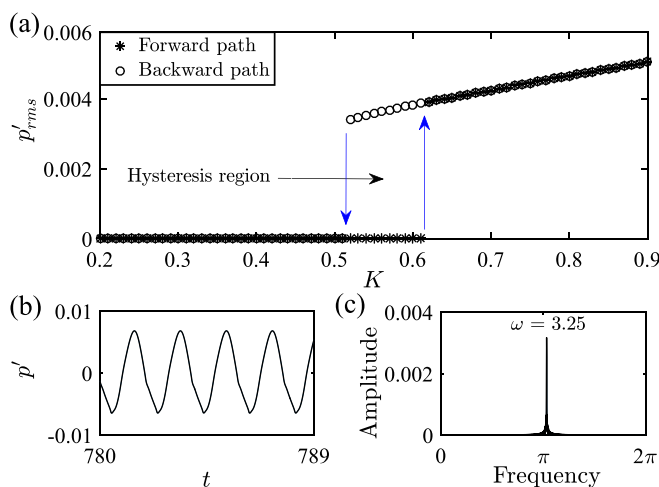


FIG. 1. (a) Bifurcation diagram showing the variation of non-dimensional  $p'_{rms}$  with non-dimensional heater power ( $K$ ). In the forward path, we observe a Hopf bifurcation point around  $K_{Hopf} = 0.62$ . However, in the reverse path, the bifurcation happens through fold point around  $K_{fold} = 0.52$ . (b) The waveform and (c) amplitude spectrum of the acoustic pressure signal corresponding to  $K = 0.75$  (a state of limit cycle oscillation) are shown. For the given set of parameter values, we observe a dominant peak in non-dimensional frequency around  $\omega = 3.25$ .

frequency [ $\omega = 3.25$  in Fig. 1(c)]. When the value of  $K$  is reduced in the reverse path, a fold bifurcation happens at a lower value of  $K$  ( $K_{fold} = 0.52$ ) than  $K_{Hopf}$ . This results in a bistable (hysteresis) region, which is the characteristic of sub-critical Hopf bifurcation,<sup>37</sup> as can be seen from Fig. 1(a).

The study by Balasubramanian *et al.*<sup>34</sup> is taken as the reference for choosing the values of constants involved in Eq. (14). The resulting set of equations, Eqs. (10) and (11) along with Eqs. (13) and (14) gives the time evolution equations of the system dynamics.

Let the superscripts “ $a$ ” and “ $b$ ” denote the first and second Rijke tubes, which are coupled through both time-delay and dissipative couplings as shown in Fig. 2. Now, the modified governing equations for the first Rijke tube oscillator are as shown below:

$$\begin{aligned} \frac{d\dot{\eta}_j^a}{dt} &= \dot{\eta}_j^a, \quad (15) \\ \frac{d\dot{\eta}_j^a}{dt} + 2\zeta_j\omega_j\dot{\eta}_j^a + \omega_j^2\eta_j^a &= -j\pi K^a \left[ \sqrt{\left| \frac{1}{3} + u_f^a(t - \tau_1) \right|} - \sqrt{\frac{1}{3}} \right] \sin(j\pi x_f) \\ &\quad + \underbrace{\mathcal{K}_d(\dot{\eta}_j^b - \dot{\eta}_j^a)}_{\text{Dissipative coupling}} + \underbrace{\mathcal{K}_\tau(\dot{\eta}_j^b(t - \tau) - \dot{\eta}_j^a(t))}_{\text{Time-delay coupling}}. \quad (16) \end{aligned}$$

The governing equations for the second Rijke tube oscillator can be obtained by flipping the superscripts “ $a$ ” and “ $b$ ” in the above differential equations. The second and third terms on the right-hand side of Eq. (16) are the dissipative and time-delay coupling terms, respectively. Inserting  $\mathcal{K}_\tau = 0$  reduces the dynamical system to dissipatively coupled oscillators, while  $\mathcal{K}_d = 0$  yields time-delay coupled ones. The four parameters which are varied in the model to

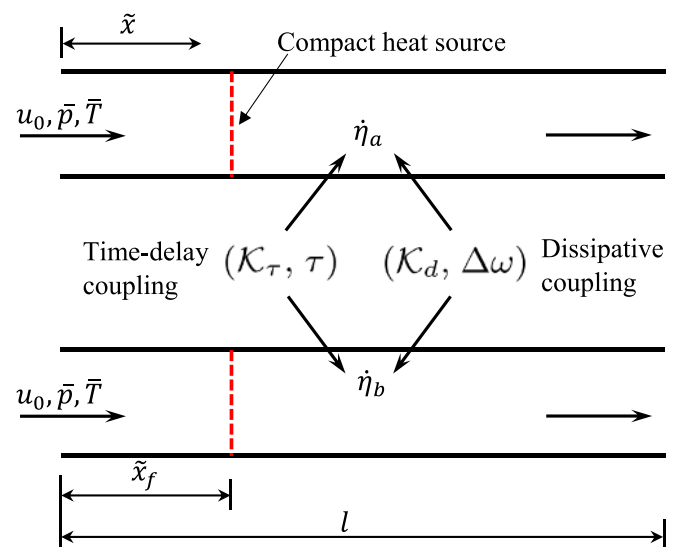


FIG. 2. A simplified illustration of the two coupled Rijke tube oscillators (named as “ $a$ ” and “ $b$ ”) subjected to both dissipative ( $\mathcal{K}_d, \Delta\omega$ ) and time-delay ( $\mathcal{K}_\tau, \tau$ ) couplings. The time varying coefficient,  $\dot{\eta}$ , of the acoustic pressure term is the variable being coupled. The flow direction is from left to right and the compact heat source is a single cylindrical wire, shown by red dashed lines.

study their effect on AD are dissipative coupling strength ( $\mathcal{K}_d$ ), time-delay coupling strength ( $\mathcal{K}_\tau$ ), detuning ( $\Delta\omega = |\omega_a - \omega_b|$ ), and delay time ( $\tau$ ). In all the simulations performed in this study, the quantities  $\omega_b/\omega_a$  ( $\omega_a$  and  $\omega_b$  being the natural frequencies of the first and the second Rijke tube oscillators, respectively, where  $\omega = 2\pi f$ ,  $f$  being the frequency) and  $\Delta\omega$  are varied by keeping  $\omega_a$  constant at 3.25 [determined from the fast Fourier transform of the pressure time series, Fig. 1(c)] and varying  $\omega_b$ .

The ODEs given in Eqs. (15) and (16) are solved numerically using the fourth order Runge-Kutta scheme, and  $p'$  and  $u'$  are calculated from Eqs. (8) and (9), respectively.

### III. RESULTS AND DISCUSSIONS

In this section, we demonstrate the effect of two types of couplings, namely, time-delay and dissipative coupling, on the occurrence of AD in the system of two coupled thermoacoustic oscillators. We first demonstrate the effect of individual coupling on the occurrence of AD in both the oscillators and then study the case where they are applied simultaneously. The results are summarized in the bifurcation plots. In the one-parameter bifurcation plot, a root mean square value of the acoustic pressure oscillations ( $p'_{rms}$ ) is plotted as a function of one of the parameters (e.g., time delay,  $\tau$ ) which is varied. The value of  $p'_{rms}$  is calculated when the transients are over and the acoustic pressure oscillations achieve an asymptotic state after the application of coupling.

In the two-parameter bifurcation plot, the variation of the coupling strength required to achieve AD is plotted as a function of the corresponding coupling parameter—delay time or detuning. While the one-parameter bifurcation plot helps in detecting the transition points of both oscillators from limit cycle oscillations (LCO) to AD state, the two-parameter bifurcation plot aids in depicting the regions of AD in the system dynamics for a given range of the parameter values.

#### A. Effect of time-delay coupling

First, we analyze the effect of time-delay coupling alone, i.e., when  $\mathcal{K}_d = 0$ , on the system of two identical

( $\Delta\omega = 0$ ) thermoacoustic oscillators (Fig. 3). Coupling in majority of the physical systems involves time-delay, due to the finite time a signal needs to travel from one system to the other. When two conservative systems are coupled through the first time-derivative of the variable involved in the governing equations ( $\dot{\eta}$  or equivalently acoustic pressure in the case of Rijke tube oscillators) with delay, they can exhibit AD.<sup>14</sup> Physically, in the system considered here, the coupling strength and delay time may be varied by changing the diameter and length, respectively, of the tube that couples the two Rijke tube oscillators. Ideally, if the length of the connecting tube is zero, there will be no delay between the signals from the two oscillators. In such a case, the oscillators are said to be dissipatively coupled.

Figures 3(a) and 3(b) are two representative plots showing the effect of time-delay coupling on the amplitude of acoustic pressure signal acquired from one of the oscillators. Since the thermoacoustic oscillators considered in this case are identical, and the coupling between them is symmetric, the variation of acoustic pressure exhibited by these oscillators is also identical. In both the cases [Figs. 3(a) and 3(b)], the non-dimensional heater power in both Rijke tubes ( $K^a = K^b = K$ ) is maintained constant at 0.92. This value of  $K$  is chosen because it is sufficiently higher than the  $K$  value corresponding to the Hopf point ( $K_{Hopf} = 0.62$ ) for the individual Rijke tube oscillators.<sup>37</sup> In these two figures, the time-delay coupling strength ( $\mathcal{K}_\tau$ ) is the sole parameter varied across the two cases, other parameters being kept constant: non-dimensional delay time ( $\tau = 0.5$ ), dissipative coupling constant ( $\mathcal{K}_d = 0$ ), and detuning ( $\Delta\omega = 0$ ).

Figure 3(a) shows the case where the coupling strength between the two Rijke tube oscillators is not strong enough ( $\mathcal{K}_\tau = 0.04$ ) to achieve AD. We observe that the amplitude of the LCO shows a small decrease from the instant where the coupling is applied, before saturating to another steady state value. On the other hand, when the coupling is strong enough ( $\mathcal{K}_\tau = 0.2$ ) to achieve AD [Fig. 3(b)], the amplitude of LCO of the acoustic pressure ( $p'$ ) decays exponentially to a zero value, once the coupling is applied. We show a one-parameter bifurcation plot in Fig. 3(c) that shows the

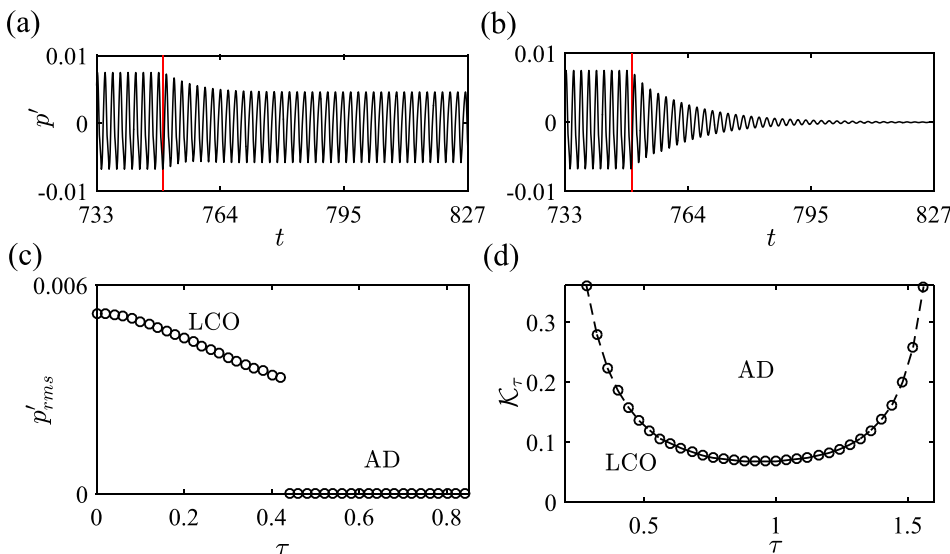


FIG. 3. The temporal variation of non-dimensional acoustic pressure ( $p'$ ), when time-delay coupling between the two oscillators is (a) not strong enough ( $\mathcal{K}_\tau = 0.04$  and  $\tau = 0.5$ ) and (b) strong enough ( $\mathcal{K}_\tau = 0.2$  and  $\tau = 0.5$ ) to achieve AD. The vertical line (shown in red) indicates the instant at which coupling is applied. (c) One-parameter bifurcation plot showing the variation of  $p'_{rms}$  with  $\tau$  ( $\mathcal{K}_\tau = 0.16$ ). (d) Two-parameter bifurcation diagram in the parameter plane of time-delay coupling strength ( $\mathcal{K}_\tau$ ) and delay time ( $\tau$ ) showing the region of AD. For all plots,  $\mathcal{K}_d = 0$ ,  $\Delta\omega = 0$ , and  $K^a = K^b = 0.92$ .

variation of  $p'_{rms}$  with  $\tau$  for one of the Rijke tube oscillators while the time-delay coupling strength is held constant ( $\mathcal{K}_\tau = 0.24$ ). We observe that the bifurcation of LCO to AD happens around  $\tau = 0.4$ , where the  $p'_{rms}$  value of LCO suddenly falls to zero. We further notice that, prior to the bifurcation, when the delay is not sufficient to achieve AD for the given value of  $\mathcal{K}_\tau$ , the amplitude of LCO continuously reduces by a small value with increase in  $\tau$ . A qualitatively similar bifurcation plot is obtained when  $\tau$  is kept constant and the value of  $\mathcal{K}_\tau$  is varied [shown in the [supplementary material](#), Fig. S1(a)].

The effect of time-delay coupling on AD characteristics of two identical thermoacoustic oscillators is further studied using a two-parameter bifurcation plot [Fig. 3(d)] in which the time-delay coupling strength ( $\mathcal{K}_\tau$ ) required to achieve AD is plotted against delay time ( $\tau$ ). The bifurcation diagram turns out to be a U-shaped plot in the range of parameter values considered. The  $\mathcal{K}_\tau - \tau$  combinations which lie inside the U-shaped plot exhibit AD, while those lying outside do not. The points indicated by the markers along the U-shape are the points where bifurcation occurs from LCO to AD. These points correspond to the smallest coupling strength, at a particular  $\tau$ , for which AD occurs in the dynamics of both the oscillators.

From Fig. 3(d), we observe that AD most easily occurs around  $\tau = 0.94$ . This corresponds to a value of  $\omega\tau$  close to  $\pi$ . Although in most of the previous studies<sup>14,44</sup> on mutually

coupled oscillators, AD was most favoured around  $\omega\tau = \pi/2$ , this is not the same in the present study. Achieving AD near  $\omega\tau = \pi$  might be a characteristic of the specific system we study. Furthermore, in other studies on closed-loop forcing of thermoacoustic oscillations, a phase delay of  $\pi$  has been implemented as a strategy of active control in thermoacoustic systems.<sup>27</sup> In such cases, reduction in the amplitude has been found due to the negative feedback between self-sustained oscillations and phase-lagged oscillations of the feedback signal. This might be a reason behind the observation of AD region around the phase delay of  $\pi$  when time-delay coupling alone is implemented in our system. However, the precise reason behind achieving AD around  $\omega\tau = \pi$  in coupled Rijke tube oscillators needs further investigation.

## B. Effect of dissipative coupling

Now, we study the effect of dissipative coupling alone (for  $\mathcal{K}_\tau = 0$ ) on the coupled behaviour of the system of two non-identical ( $\Delta\omega \neq 0$ ) Rijke tube oscillators (Fig. 4). We observe that, when  $\mathcal{K}_d$  is not high enough ( $\mathcal{K}_d = 0.1$ ) to reach AD state, the amplitude of LCO of both the oscillators reduces a bit and oscillates around this reduced value once the coupling is applied [see Fig. 4(a)]. At this state, the oscillations of both oscillators show a beat like behaviour, because of the interaction between the two oscillators with

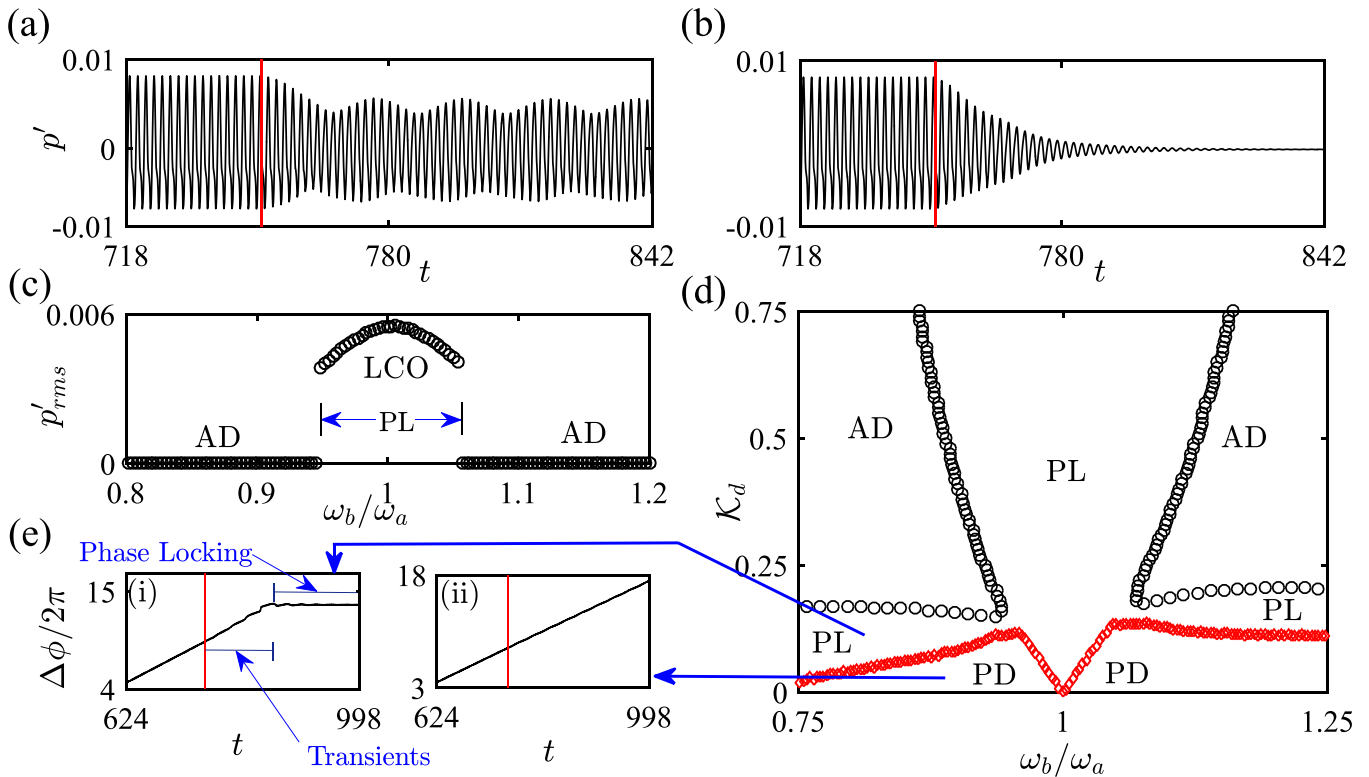


FIG. 4. The temporal variation of non-dimensional acoustic pressure ( $p'$ ), when the dissipative coupling between the two oscillators is (a) not strong enough ( $\mathcal{K}_d = 0.1$  and  $\Delta\omega = 0.24$ ) and (b) strong enough ( $\mathcal{K}_d = 0.3$  and  $\Delta\omega = 0.24$ ) to achieve AD, respectively. (c) One-parameter bifurcation plot showing the variation of  $p'_{rms}$  with  $\omega_b/\omega_a$  ( $\mathcal{K}_d = 0.18$ ). (d) Two-parameter bifurcation diagram in the parameter plane of dissipative coupling strength ( $\mathcal{K}_d$ ) and ratio of natural frequencies ( $\omega_b/\omega_a$ ), showing regions of AD, phase locking (PL), and phase drifting (PD). Circles (in black) indicate the boundary between AD and PL region, while diamonds (in red) mark the boundary between PL and PD. (e) Phase plots showing the variation of relative phase ( $\Delta\phi$ ) between the two oscillators for (i) PL region and (ii) PD region. Note that phase locking in (e-i) follows a small interval of transients wherein the signals show phase drifting behaviour. The vertical lines (shown in red) in (a), (b), and (e) indicate the instant at which coupling is applied. For all the plots,  $\mathcal{K}_\tau = 0$  and  $K^a = K^b = 1.02$ .

two different but close by frequencies. However, when the  $\mathcal{K}_d$  value is high enough ( $\mathcal{K}_d = 0.3$ ) to achieve AD, amplitude of both the oscillators dies down after the application of coupling [Fig. 4(b)]. In Fig. 4(c), we plot a one-parameter bifurcation plot that shows the variation of  $p'_{rms}$  with the ratio of natural frequencies ( $\omega_b/\omega_a$ ) of the two Rijke tube oscillators, while the dissipative coupling strength ( $\mathcal{K}_d$ ) between them is kept constant at 0.18. We observe from Fig. 4(c) that it is impossible to achieve AD through dissipative coupling alone, when the natural frequencies of the two oscillators are very close by. In the current case with the given dissipative coupling strength ( $\mathcal{K}_d = 0.18$ ), oscillations were observed in the range of  $\omega_b/\omega_a$  values from 0.95 to 1.05, and AD on either sides. We obtain a second one-parameter bifurcation plot [shown in [supplementary material](#), Fig. S1(b)], qualitatively similar to that in Fig. 3(c), when  $\omega_b/\omega_a$  is kept constant at 0.93 (or  $\Delta\omega = 0.24$ ) and the value of  $\mathcal{K}_d$  is varied.

Further, we illustrate the regions of AD in the parameter plane of  $\mathcal{K}_d$  and  $\omega_b/\omega_a$ , when time-delay coupling is absent in the system of two Rijke tube oscillations, i.e.,  $\mathcal{K}_\tau = 0$  [Fig. 4(d)]. In Fig. 4(d), the circular (in black) and diamond (in red) markers correspond to the points where bifurcation from phase locking (PL) to AD and phase drifting (PD) to PL occur, respectively. Phase drifting is said to occur between two oscillators, when the relative phase between them is unbounded and exhibit an increase with time. On the other hand, phase locking is the scenario where the relative phase between the oscillators is bounded. For those combinations of  $\mathcal{K}_d$  and  $\omega_b/\omega_a$  values which are segregated solely by the curve with circular markers, AD will occur, and for other combinations of  $\mathcal{K}_d$  and  $\omega_b/\omega_a$  values, AD is not observed. In the region amidst the curves with circular and diamond markers, the relative phase between the two oscillators will become locked after the coupling is applied [Fig. 4(d)].

The relative phase dynamics with one such combination of  $\mathcal{K}_d$  and  $\omega_b/\omega_a$  in the PL region is shown in Fig. 4(e-i). However, this phase locking follows a small interval of phase drifting after the application of coupling, owing to the transients [Fig. 4(e-i)]. In contrast, phase drifting happens in the region below the curve with diamond markers [Fig. 4(d)]. The relative phase dynamics with a combination of  $\mathcal{K}_d$  and  $\omega_b/\omega_a$  in the PD region is shown in Fig. 4(e-ii).

Therefore, we infer that, as the coupling strength between the two oscillators is increased, the system moves from phase drifting to phase locking (or synchronization) and then to AD. However, when the natural frequencies of the two oscillators are very close by, even very high values of coupling strength are not sufficient to achieve AD, as can be seen from the range of  $\omega_b/\omega_a$  values around 1 (0.93 to 1.08) in Fig. 4(d). This is in accordance with the earlier literature on AD,<sup>32,35</sup> which states that there should be a sufficient difference between the frequencies of the two oscillators for a purely dissipative coupling to bring about AD. However, phase locking easily happens in the region of  $\omega_b/\omega_a$  values around 1 as the frequency values of the two oscillators are already very close. Furthermore, the zone of phase locking in the range of  $\omega_b/\omega_a$  values around 1 becomes wider as we increase the coupling strength, which

is similar to the experimental observation reported by Biwa *et al.*<sup>32</sup>

Further, we note that the bifurcations observed in Fig. 4(d) are different from the bifurcation diagram plotted in the parameter space of  $\phi$  (analogous to dissipative coupling strength) and  $\Delta f$  (frequency detuning, corresponding to  $\Delta\omega$  in the present study) by Biwa *et al.*<sup>32</sup> In their study, the transitions are (i) from phase drifting (PD) to phase locking (PL) through AD when  $\Delta f$  is sufficiently large and (ii) a direct transition from PD to PL when  $\Delta f$  is small. In contrast, we observe the transitions (i) from phase drifting (PD) to amplitude death (AD) through phase locking (PL) when the value of  $\omega_b/\omega_a$  is away from 1, and (ii) direct transition from PD to PL when the value of  $\omega_b/\omega_a$  is close to 1. We believe that this dissimilarity in the first transition could be due to the difference in the underlying mechanisms which lead to the onset of self-sustained oscillations in the two systems.

### C. Effect of simultaneous application of time-delay and dissipative coupling

We now consider the effect of simultaneous application of time-delay and dissipative couplings on the regions of AD in the two-parameter bifurcation plots. Here, the non-dimensional heater power for both the Rijke tube oscillators ( $K^a = K^b = K$ ) is kept constant. The bifurcation diagrams in the parameter plane constituted by  $\mathcal{K}_\tau$  and  $\tau$  shown in Fig. 5(a) represent the case where dissipative coupling is applied to a system which is already coupled through time-delay. The bifurcation plot when time-delay coupling alone is applied on a system of two identical oscillators is shown in Fig. 5(a-i) for comparison, while in Figs. 5(a-ii) to 5(a-iv), the oscillators are non-identical. We see that the introduction of detuning ( $\Delta\omega = 0.24$ ) between the oscillators results in the splitting of the AD region into 3 unequal regions, even when  $\mathcal{K}_d = 0$ , as shown in Fig. 5(a-ii). This change in regions of AD can have practical implications. In practice, for a set of seemingly identical oscillators, we expect them to give rise to AD for a certain set of parameter values, as indicated in Fig. 5(a-i). However, we may not achieve AD in such cases with the given set of parameter values, because of the inherent detuning ( $\Delta\omega \neq 0$ ) between the oscillators (Fig. 5(a-ii). At this detuning ( $\Delta\omega = 0.24$ ) when dissipative coupling is introduced ( $\mathcal{K}_d = 0.05$ ), we notice the merging of these separated AD zones into a single W-shaped region as seen in Fig. 5(a-iii). Finally, with further increase in  $\mathcal{K}_d$ , the central W-shaped region becomes more flattened, resulting in the appearance of a single unsymmetric U-shaped region in the two-parameter plane, as can be seen from Fig. 5(a-iv).

We further show the effect of applying time-delay coupling to a system which is already coupled through dissipative coupling in Fig. 5(b). The regions of AD in the two-parameter bifurcation plot in the parameter plane of  $\mathcal{K}_d$  and  $\omega_b/\omega_a$  is affected as a consequence of adding time-delay coupling. The circular markers correspond to the case where dissipative coupling alone is applied to the system. As the time-delay coupling strength applied on the oscillators is increased, the graphs shift downward and the region near the  $\omega_b/\omega_a$  value of 1, where AD is unattainable, narrows down.

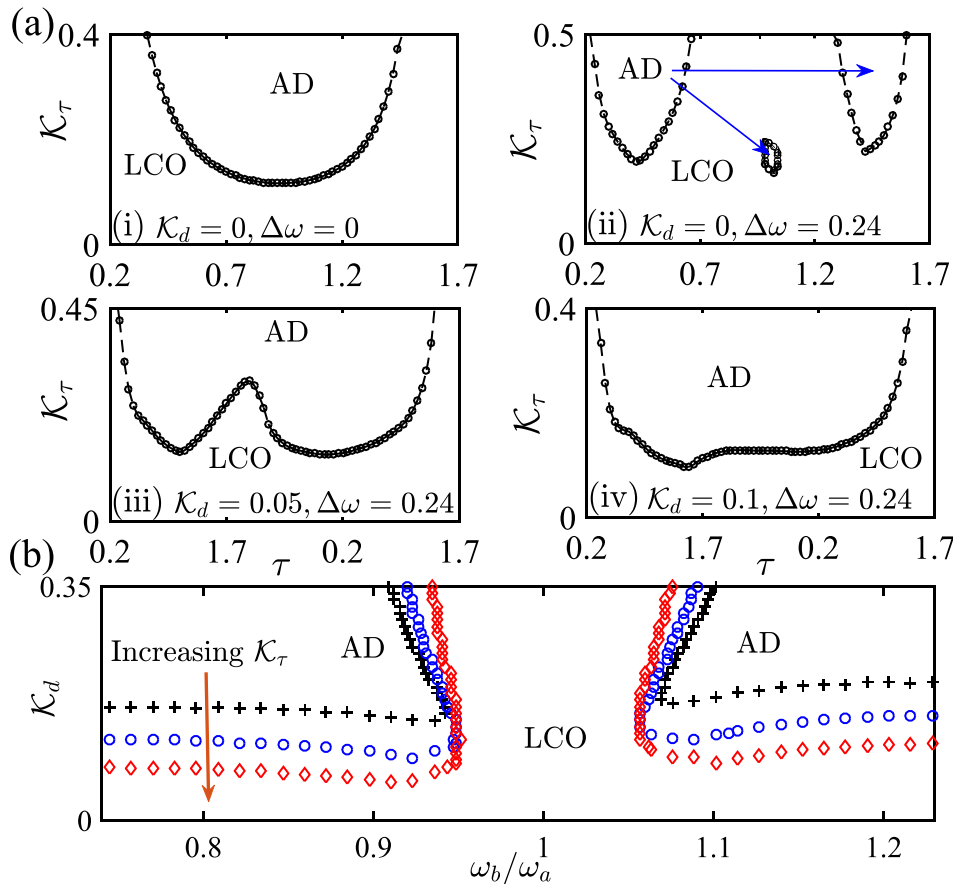


FIG. 5. Two-parameter bifurcation diagram in the parameter plane of (a)  $\mathcal{K}_\tau$  and  $\tau$ , when (i)  $\mathcal{K}_d = 0, \Delta\omega = 0$ ; (ii)  $\mathcal{K}_d = 0, \Delta\omega = 0.24$ ; (iii)  $\mathcal{K}_d = 0.05, \Delta\omega = 0.24$ ; and (iv)  $\mathcal{K}_d = 0.1, \Delta\omega = 0.24$ . (b)  $\mathcal{K}_d$  and  $\omega_b/\omega_a$  for three different  $\mathcal{K}_\tau$  values keeping the value of  $\tau$  constant at 0.5: Plus— $\mathcal{K}_\tau = 0$ ; Circle— $\mathcal{K}_\tau = 0.04$ ; Diamond— $\mathcal{K}_\tau = 0.08$ .

The values of  $\tau = 0.5$  and  $\mathcal{K}_\tau = 0.04$  and  $0.08$  are chosen such that the system does not exhibit AD with time-delay coupling alone. We can conclude that the  $\mathcal{K}_d$  value needed for the bifurcation of LCO to AD is smaller in the presence of a small value of time-delay coupling, which alone is not sufficient to bring about AD, than in the case where dissipative coupling alone is applied. These trends from Fig. 5(b) make it evident that simultaneous application of both the couplings makes it easier to achieve AD. Please note that we focus on the occurrence of AD from Fig. 5 onward. Therefore, unlike Fig. 4, we do not distinguish PL and PD so as not to clutter the plots.

#### D. Effect of amplitude of oscillations on AD phenomenon

Another factor which decides if a certain set of coupling parameters can lead the system to AD is the amplitude of limit cycle oscillations. The amplitude of acoustic pressure oscillations in a Rijke tube can be controlled using the heater power value. In the model, this is achieved by changing the non-dimensional heater power value ( $K$ ). An increase in  $K$  value will result in an increase in the amplitude of the LCO.<sup>43</sup> The two-parameter bifurcation plots in two different parameter planes ( $\mathcal{K}_d$  versus  $\omega_b/\omega_a$  and  $\mathcal{K}_\tau$  versus  $\tau$ ), for three different values of the heater power ( $K$ ), are shown in Figs. 6(a) and 6(b), respectively. Note that the values of heater power in both Rijke tube oscillators are changed in an identical manner (i.e.,  $K^a = K^b$ ). When dissipative coupling alone is applied on this system, an increase in  $K$  results in

the bifurcation plot moving up, as shown in Fig. 6(a). Also, the region near the  $\omega_b/\omega_a$  value of 1, where AD is not observed, becomes wider. In a similar fashion, when time-delay coupling alone is applied, the U-shaped bifurcation plot shifts up and becomes narrower as we increase the  $K$  value [Fig. 6(b)]. As the amplitude of oscillations increases with an increase in heater power value, we infer from the Figs. 6(a) and 6(b) that the higher the amplitude of oscillations, the higher the coupling strength needed at a certain value of time-delay or detuning to achieve AD. This also suggests that the size of the region of AD in the parameter planes decreases with increase in the amplitude of LCO.

#### E. AD phenomenon when two oscillators of different amplitudes are coupled

All the coupling scenarios we studied above are for two oscillators with identical amplitudes of the LCO. In practical conditions, the coupled oscillators might be oscillating with considerably dissimilar amplitudes. Such a situation can be explored by controlling the  $K$  values of individual Rijke tube oscillators in the model. We consider the case where two Rijke tube oscillators with significantly different limit cycle amplitudes of their acoustic pressure oscillations are coupled through time-delay alone. In Figs. 7(a) and 7(b), we fix the heater power value ( $K^a = 0.72$ ) of the Rijke tube “a” and show the effect of two different heater power values of Rijke tube “b” ( $K^b$ ) at a particular coupling strength ( $\mathcal{K}_\tau = 0.4$ ). We choose high values of  $K^b$  compared to  $K^a$  in both cases [Figs. 7(a) and 7(b)] to realize a considerable amplitude

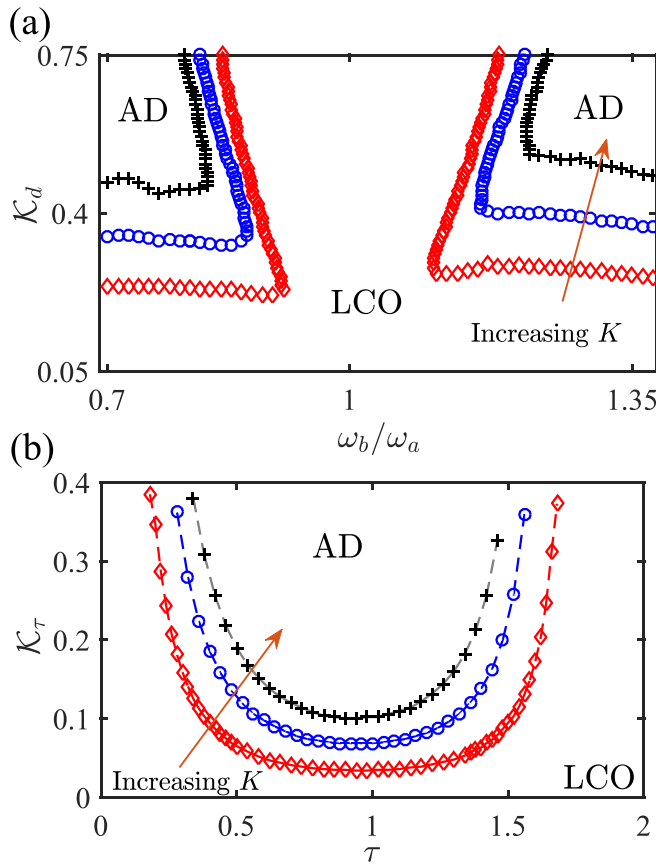


FIG. 6. Two-parameter bifurcation diagrams for different values of  $K$  ( $K^a = K^b$ ) in the parameter plane of (a)  $\mathcal{K}_d$  and  $\omega_b/\omega_a$ , where diamond, circle, and plus markers correspond to  $K$  values of 1.22, 1.52, and 1.82, respectively. (b)  $\mathcal{K}_\tau$  and  $\tau$ , where diamond, circle, and plus markers correspond to  $K$  values of 0.72, 0.92, and 1.12, respectively.

difference between the two oscillators. These high values of heater power ( $K^b$ ) cause period doubling of the limit cycle oscillations in the Rijke tube “*b*.” Therefore, in both the cases, we are coupling the period-2 LCO in Rijke tube “*b*” with the period-1 LCO in “*a*.” The occurrence of period-2 limit cycle oscillations with a high value of  $K$  has been reported earlier in the study by Subramanian *et al.*<sup>37</sup> using the same model and by Gopalakrishnan *et al.*<sup>45</sup> in experiments. In this study, the purpose of using a high value of  $K$  is to create very high amplitude oscillations in one of the Rijke tube oscillators. One may need great care to design such a system to ensure that the heater does not melt at such high values of heater power. However, the effect of period-2 dynamics on the AD phenomena was not our focus and needs further investigation.

Figure 7(a) shows the instance where low amplitude oscillations in Rijke tube “*a*” are coupled with high amplitude oscillations in “*b*,” resulting in a complete cessation of oscillations in both. The amplitude of oscillations (or equivalently the  $K^b$  value) in Rijke tube “*b*” is further increased in Fig. 7(b). We observe that, after the coupling is applied, the LCO amplitude of the second Rijke tube oscillator “*b*” reduces considerably and then remains constant at this reduced value. The interesting phenomena observed here is that, even when this particular coupling strength is not strong enough to bring about AD, we could still suppress the very

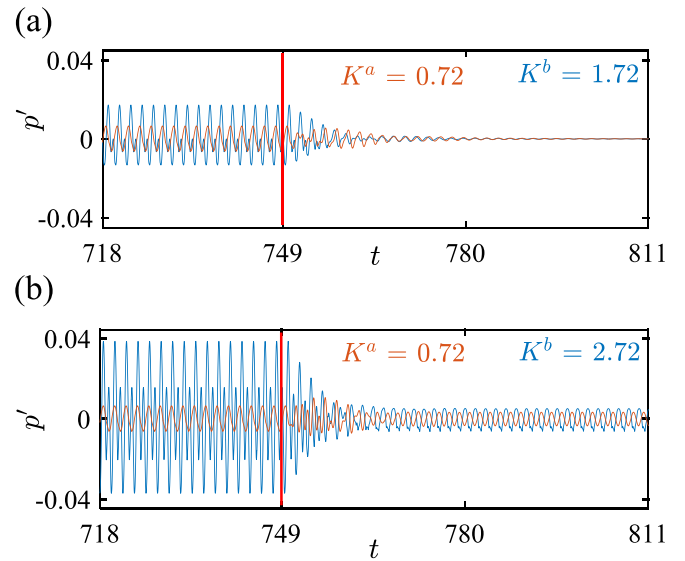


FIG. 7. Temporal variation of non-dimensional acoustic pressure ( $p'$ ) in both the coupled oscillators (for  $K^a \neq K^b$ ), when (a) AD is attained ( $K^b = 1.72$ ) and (b) AD is not attained ( $K^b = 2.72$ ), while keeping the value of  $K^a$  constant at 0.72. The orange and blue time series correspond to the oscillators “*a*” and “*b*,” respectively. The other fixed parameters are  $\tau = 0.4$ ,  $\mathcal{K}_\tau = 0.4$ ,  $\Delta\omega = 0$ , and  $\mathcal{K}_d = 0$ . The vertical line (shown in red) indicates the instant at which coupling is applied.

high amplitude oscillations in Rijke tube “*b*” considerably with the low amplitude oscillations in Rijke tube “*a*.” After the application of coupling, the oscillation amplitude of the high amplitude oscillator becomes almost as low as that in the low amplitude one.

## F. Effect of asymmetrical coupling on AD phenomenon

Further, we try to understand the effect of asymmetrical coupling on the coupled dynamics of the two Rijke tube oscillators. A system of two oscillators is said to be asymmetrical coupling when the coupling strength as perceived by the two oscillators is different, which may be the case in many practical systems. We use symmetry parameters  $n$  ( $0 \leq n \leq 1$ ) and  $m$  ( $0 \leq m \leq 1$ ) to bring in asymmetry to the coupled Rijke tube oscillator model as shown below:

$$\mathcal{K}_d^a = n\mathcal{K}_d; \quad \mathcal{K}_d^b = (1-n)\mathcal{K}_d, \quad (17)$$

$$\mathcal{K}_\tau^a = m\mathcal{K}_\tau; \quad \mathcal{K}_\tau^b = (1-m)\mathcal{K}_\tau. \quad (18)$$

Two-parameter bifurcation diagram in which  $\mathcal{K}_\tau$  required to attain AD is plotted against  $m$ , in the range of  $m$  values from 0 to 0.5, is shown in Fig. 8(a).

We observe that, the  $\mathcal{K}_\tau$  value needed to attain AD increases with an increase in the asymmetry in the coupling. This increase is very marginal when asymmetry is less (in the range of  $m$  values from 0.5 to 0.25), but becomes very sharp as  $m$  approaches zero. When the variation of  $\mathcal{K}_\tau$  with  $m$  is plotted in the log-log scale, we obtained a straight line, which indicates that there exists a power law relation between the smallest  $\mathcal{K}_\tau$  value required to achieve AD and the asymmetry parameter ( $m$ ). This implies that the oscillatory behavior of the system is not affected gradually, but in

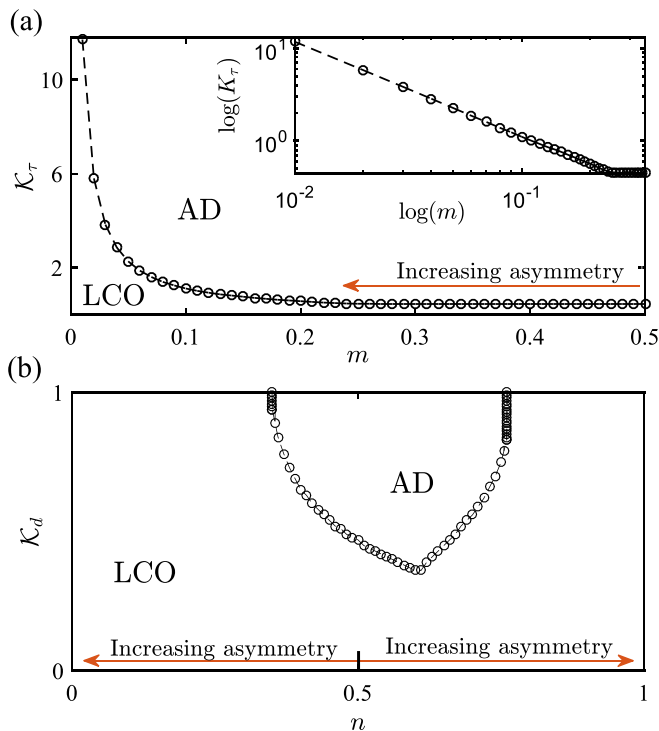


FIG. 8. Two-parameter bifurcation diagram in the parameter plane of (a)  $\mathcal{K}_\tau$  and  $m$ , where the upper right inset shows the fit in the log-log plot, which turns out to be a straight line—indicating a power law relation. The parameters that are held fixed are  $\tau = 0.5$ ,  $\Delta\omega = 0$ , and  $\mathcal{K}_d = 0$ . (b)  $\mathcal{K}_d$  and  $n$ , where  $\mathcal{K}_\tau$  value is fixed at 0 and  $\Delta\omega = 0.55$ .

an exponential manner when the asymmetry in the time-delay coupling is varied. Further studies need to be done to understand the physics behind this power law relation. Figure 8(a) will be symmetrical about  $m = 0.5$ , as increasing the  $m$  value beyond 0.5 is equivalent to interchanging the two identical oscillators. In other words, the degree of asymmetry for the identical oscillators essentially increases in the same manner, as we move away from 0.5 in either directions. The combinations of  $\mathcal{K}_\tau$  and  $m$  values for an asymmetrically coupled system, which can lead to AD are those which lie above the curve. We see that there is only negligible increase in the  $\mathcal{K}_\tau$  values required to attain AD around  $m = 0.5$  to 0.2 [Fig. 8(a)]. Therefore, the model for symmetrical coupling is sufficient to predict the time-delay coupling strength required to attain AD even in practical coupled oscillators, where slight asymmetry is bound to occur.

We also analyze the effect of asymmetry in dissipative coupling alone on the system of two coupled Rijke tube oscillators. Figure 8(b) represents the two-parameter bifurcation diagram in parameter plane of  $\mathcal{K}_d$  and  $n$ . However, we notice that asymmetry in dissipative coupling does not seem to exhibit a power law behavior as in the case of time-delay coupling [Fig. 8(a)]. Further, AD is attained only in the range of  $n$  values around 0.35 to 0.76 (for,  $\Delta\omega = 0.55$ ). Also, it is important to note that this plot is not symmetrical about  $n = 0.5$ , as the two coupled oscillators are nonidentical. Since there are two different frequencies associated with the two oscillators, increasing the  $m$  value beyond 0.5 is not equivalent to interchanging the oscillators.

## IV. CONCLUSION

We explored the effect of time-delay and dissipative couplings on the occurrence of amplitude death phenomenon in a system of two coupled thermoacoustic oscillators known as horizontal Rijke tubes. Bifurcation plots obtained from the mathematical model give us an idea about the combination of coupling parameters that need to be set to achieve AD in the thermoacoustic oscillators considered. The results indicate that AD is more easily achieved when both the couplings are applied together. The fact that theoretically AD is possible under asymmetric coupling and in coupled oscillators with dissimilar amplitudes is also demonstrated. This phenomenon of AD in the Rijke tube oscillator model, if found experimentally feasible, can be extended to real combustion systems where the unwanted high amplitude oscillations which may lead to a serious structural damage can be inhibited. The theoretical finding that AD can occur even in oscillators with considerably dissimilar amplitudes also needs experimental verification in practical thermoacoustic systems.

## SUPPLEMENTARY MATERIAL

See [supplementary material](#) for the one parameter bifurcation plots showing variation of  $p'_{rms}$  with coupling strengths  $\mathcal{K}_\tau$  and  $\mathcal{K}_d$  separately.

## ACKNOWLEDGMENTS

S.M. gratefully acknowledges the Institute Post-doctoral Fellowship of IIT Madras. This work was supported by Office of Naval Research Global (Contract Monitor: Dr. R. Kolar).

- <sup>1</sup>P. C. Matthews and S. H. Strogatz, *Phys. Rev. Lett.* **65**, 1701 (1990).
- <sup>2</sup>A. Pikovsky, M. Rosenblum, and J. Kurths, *Synchronization: A Universal Concept in Nonlinear Sciences* (Cambridge University Press, 2003), Vol. 12.
- <sup>3</sup>Y. Kuramoto, *Prog. Theor. Phys. Suppl.* **79**, 223 (1984).
- <sup>4</sup>R. Herrero, M. Figueras, J. Rius, F. Pi, and G. Orriols, *Phys. Rev. Lett.* **84**, 5312 (2000).
- <sup>5</sup>D. R. Reddy, A. Sen, and G. L. Johnston, *Phys. Rev. Lett.* **80**, 5109 (1998).
- <sup>6</sup>R. E. Mirolo and S. H. Strogatz, *J. Stat. Phys.* **60**, 245 (1990).
- <sup>7</sup>A. Koseska, E. Volkov, and J. Kurths, *Phys. Rev. Lett.* **111**, 024103 (2013).
- <sup>8</sup>J. W. S. Rayleigh, *The Theory of Sound* (Dover, 1945).
- <sup>9</sup>M. Abel, S. Bergweiler, and R. Gerhard-Multhaupt, *J. Acoust. Soc. Am.* **119**, 2467 (2006).
- <sup>10</sup>M. Abel, K. Ahnert, and S. Bergweiler, *Phys. Rev. Lett.* **103**, 114301 (2009).
- <sup>11</sup>M. F. Crowley and R. J. Field, *Nonlinear Phenomena in Chemical Dynamics* (Springer, 1981), pp. 147–153.
- <sup>12</sup>K. P. Zeyer, M. Mangold, and E. Gilles, *J. Phys. Chem. A* **105**, 7216 (2001).
- <sup>13</sup>Y. Setou, Y. Nishio, and A. Ushida, *IEICE Trans. Fundam. Electron., Commun. Comput. Sci.* **79**, 1575 (1996).
- <sup>14</sup>G. Saxena, A. Prasad, and R. Ramaswamy, *Phys. Rep.* **521**, 205 (2012).
- <sup>15</sup>S. Mondal, A. Mukhopadhyay, and S. Sen, *Combust. Theor. Modell.* **16**, 59 (2012).
- <sup>16</sup>S. Mondal, A. Mukhopadhyay, and S. Sen, *Combust. Theor. Modell.* **21**, 487 (2017).
- <sup>17</sup>G. W. Swift, *J. Acoust. Soc. Am.* **84**, 1145 (1988).
- <sup>18</sup>V. R. Unni, Y. M. Prasaad, N. Ravi, S. M. Iqbal, B. Pesala, and R. Sujith, *Int. J. Spray Combust. Dyn.* **7**, 113 (2015).
- <sup>19</sup>J. W. S. Rayleigh, *Nature* **18**, 319 (1878).

- <sup>20</sup>A. A. Putnam, *Combustion Driven Oscillations in Industry* (Elsevier Publishing Company, 1971).
- <sup>21</sup>R. I. Sujith, M. Juniper, and P. Schmid, *Int. J. Spray Combust. Dyn.* **8**, 119 (2016).
- <sup>22</sup>S. C. Fisher and S. A. Rahman, *Remembering the Giants: Apollo Rocket Propulsion Development* (NASA Stennis Space Center, 2009).
- <sup>23</sup>S. J. Shanbhogue, S. Husain, and T. Lieuwen, *Prog. Energy Combust. Sci.* **35**, 98 (2009).
- <sup>24</sup>T. Poinso, *Proc. Combust. Inst.* **36**, 1 (2017).
- <sup>25</sup>M. P. Juniper and R. I. Sujith, *Annu. Rev. Fluid Mech.* **50**, 661–689 (2017).
- <sup>26</sup>A. Bicen, D. Tse, and J. Whitelaw, *Combust. Flame* **72**, 175 (1988).
- <sup>27</sup>K. McManus, T. Poinso, and S. Candel, *Prog. Energy Combust. Sci.* **19**, 1 (1993).
- <sup>28</sup>N. A. Kablar, T. Hayakawa, and W. M. Haddad, in *Proceedings of the 2001 American Control Conference* (IEEE, 2001), Vol. 3, pp. 2468–2473.
- <sup>29</sup>T. Biwa, Y. Sawada, H. Hyodo, and S. Kato, *Phys. Rev. Appl.* **6**, 044020 (2016).
- <sup>30</sup>B. D. Bellows, Y. Neumeier, and T. Lieuwen, *J. Propul. Power* **22**, 1075 (2006).
- <sup>31</sup>S. Balusamy, L. K. Li, Z. Han, M. P. Juniper, and S. Hochgreb, *Proc. Combust. Inst.* **35**, 3229 (2015).
- <sup>32</sup>T. Biwa, S. Tozuka, and T. Yazaki, *Phys. Rev. Appl.* **3**, 034006 (2015).
- <sup>33</sup>G. Ghirardo and M. P. Juniper, *Proc. R. Soc. A* **469**, 20130232 (2013).
- <sup>34</sup>K. Balasubramanian and R. I. Sujith, *Phys. Fluids* **20**, 044103 (2008).
- <sup>35</sup>D. G. Aronson, G. B. Ermentrout, and N. Kopell, *Physica D: Nonlinear Phenom.* **41**, 403 (1990).
- <sup>36</sup>K. I. Matveev, “Thermoacoustic instabilities in the Rijke tube: Experiments and modeling,” Ph.D. thesis (California Institute of Technology, 2003).
- <sup>37</sup>P. Subramanian, S. Mariappan, R. I. Sujith, and P. Wahi, *Int. J. Spray Combust. Dyn.* **2**, 325 (2010).
- <sup>38</sup>L. V. King, *Philos. Trans. R. Soc. London, Ser. A* **214**, 373 (1914).
- <sup>39</sup>M. A. Heckl, *Acta Acust. united Ac.* **72**, 63 (1990).
- <sup>40</sup>M. E. Lores and B. T. Zinn, *Combust. Sci. Technol.* **7**, 245 (1973).
- <sup>41</sup>K. I. Matveev and F. Culick, *Combust. Sci. Technol.* **175**, 1059 (2003).
- <sup>42</sup>J. Sterling and E. Zukoski, *Combust. Sci. Technol.* **77**, 225 (1991).
- <sup>43</sup>E. A. Gopalakrishnan and R. I. Sujith, *J. Fluid Mech.* **776**, 334 (2015).
- <sup>44</sup>D. R. Reddy, A. Sen, and G. L. Johnston, *Phys. Rev. Lett.* **85**, 3381 (2000).
- <sup>45</sup>E. Gopalakrishnan and R. Sujith, *Int. J. Spray Combust. Dyn.* **6**, 293 (2014).